8156–8166 *Nucleic Acids Research, 2017, Vol. 45, No. 14* *Published online 29 June 2017*
doi: 10.1093/nar/gkx566

Monomolecular G-quadruplex structures with inversion of polarity sites: new topologies and potentiality

Antonella Virgilio, Annapina Russo, Teresa Amato, Giulia Russo, Luciano Mayol, Veronica Esposito* and Aldo Galeone*

Dipartimento di Farmacia, Università degli Studi di Napoli Federico II, Via D. Montesano 49, 80131 Napoli, Italy

Received January 18, 2017; Revised June 14, 2017; Editorial Decision June 19, 2017; Accepted June 21, 2017

ABSTRACT

In this paper, we report investigations, based on circular dichroism, nuclear magnetic resonance spectroscopy and electrophoresis methods, on three oligonucleotide sequences, each containing one 3′-3′ and two 5′-5′ inversion of polarity sites, and four G-runs with a variable number of residues, namely two, three and four (mTG$_2$T, mTG$_3$T and mTG$_4$T with sequence 3′-TG$_n$T-5′-5′-TG$_n$T-3′-3′-TG$_n$T-5′-5′-TG$_n$T-3′ in which *n* = 2, 3 and 4, respectively), in comparison with their canonical counterparts (TG$_n$T)$_4$ (*n* = 2, 3 and 4). Oligonucleotides mTG$_3$T and mTG$_4$T have been proven to form very stable unprecedented monomolecular parallel G-quadruplex structures, characterized by three side loops containing the inversion of polarity sites. Both G-quadruplexes have shown an all-*syn* G-tetrad, while the other guanosines adopt *anti* glycosidic conformations. All oligonucleotides investigated have shown a noteworthy antiproliferative activity against lung cancer cell line Calu 6 and colorectal cancer cell line HCT-116 $^{p53-/-}$. Interestingly, mTG$_3$T and mTG$_4$T have proven to be mostly resistant to nucleases in a fetal bovine serum assay. The whole of the data suggest the involvement of specific pathways and targets for the biological activity.

INTRODUCTION

G-quadruplex structures are secondary conformations of nucleic acids whose constitutive unit is the G-tetrad or G-quartet. This building block consists of a square planar arrangement of four guanosines in which each base is associated to the adjacent ones through four hydrogen bonds. Stacking of two or more G-tetrad units can form larger and more stable structures. The occurring of monovalent cations, between two adjacent G-tetrads or also in the center of a G-tetrad, further contributes to the structural stability of the G-quadruplex complexes. The biological significance of these DNA structures is witnessed by their occurrence or potential formation in several regions of the human genome such as telomeres, genes promoters and transcription start sites (1). Furthermore, they can be involved in the regulation of gene expression (2–8) and telomere maintenance. However, the importance of the G-quadruplex structures is not confined to genetics and molecular biological research. In fact, thanks to their remarkable stability and variability, these structures constitute the scaffolds of several DNA aptamers with important applications in both pharmaceutics and analytics (9,10). Furthermore, considering their self-assembly properties, G-quadruplexes are often exploited in building nanostructures and in developing nanodevices (11). Soon after they were discovered, these structures were subject to several chemical modifications and conjugation with the aim to promote, stabilize and investigate a particular conformation, improve their properties and encourage the formation of high-order structures. Most of the chemical modifications proposed have concerned the replacement of one or more natural bases with base analogues, while a minor amount of modifications concerning the sugar-phosphate backbone has appeared in the literature, probably due to their higher impact on the G-quadruplex folding properties (12).

Among the sugar-phosphate backbone modifications, the introduction of 3′-3′ and/or 5′-5′ inversion of polarity sites (IPS) represents an almost 'natural' and less heavy chemical structural change, since it involves only naturally occurring deoxyribonucleotides. Several investigations have shown that the presence of 5′-5′ IPSs in tetramolecular G-quadruplex structures is able to affect the glycosidic bond of adjacent nucleosides (13–15). As far as aptamers are concerned, the effect of IPSs in the thrombin binding aptamer (TBA) sequence has been systematically investigated by replacing, one at a time, each canonical phosphodiester bond by an IPS (16). Furthermore, the introduction of IPSs in

*To whom correspondence should be addressed. Tel: +39 081678542; Email: galeone@unina.it
Correspondence may also be addressed to Veronica Esposito. Email: verespos@unina.it

the TBA has been exploited in a different way by preparing TBA analogues characterized by one or two further residues connected to the ODN ends through a 3′-3′ IPS or through both 3′-3′ and 5′-5′ IPSs, in such a way to preserve the original biologically active sequence of the parent aptamer (17,18). Some of these analogues, have shown higher affinity to thrombin, higher structural stability and improved resistance to nucleases compared to TBA. Recently, two heterochiral TBA analogues containing both 3′-3′ and/or 5′-5′ IPSs, which have been suggested adopting left-handed G-quadruplex structures, have shown antiproliferative activity (19). Therefore, while hitherto the introduction of IPSs in G-quadruplex structures has been used to improve the properties of some aptamers, the ability of IPS to invert the strand directionality and then, to give rise to G-quadruplex topologies not allowed with canonical 3′-5′ phosphodiester bonds, has not been adequately explored and properly exploited.

It is well known that, in G-quadruplex structures, the parallel arrangement of the strands is generally considered to yield the most stable conformations. As a matter of facts, short sequences, such as TG_3T (20) and TG_4T (21), have the tendency to assemble in tetramolecular parallel arrangements, while the four G-runs containing anti HIV-integrase aptamer $(GGGT)_4$ folds in a monomolecular parallel G-quadruplex structure characterized by a remarkably high thermal stability (22).

In order to expand the structural variability and the topological repertoire of the G-quadruplex structures by exploiting the presence of IPSs, we designed and synthesized three sequences, each containing three IPSs, and four G-runs with a variable number of residues, namely two, three and four (Table 1). Between the two alternatives, namely one 3′-3′ and two 5′-5′ IPSs, or one 5′-5′ and two 3′-3′ IPSs, the first one was chosen in order to endow the molecule with two longer spacers connecting G-runs and then, facilitate the strand association. All modified ODNs were proven to form G-quadruplex structures, which were investigated by NMR and CD spectroscopy and electrophoretic methods. Taking into account the antiproliferative properties shown by other G-quadruplex structures containing IPSs (19), these ODNs were also undergone to antiproliferative assay and their resistance in biological environment was evaluated. Furthermore, in most of the experiments, the behaviour of **mTG_2T**, **mTG_3T** and **mTG_4T** was compared with those of their natural counterparts **$(TG_2T)_4$**, **$(TG_3T)_4$** and **$(TG_4T)_4$**, respectively.

MATERIALS AND METHODS

Oligonucleotides synthesis and purification

The oligonucleotides in Table 1 were synthesized on a Millipore Cyclone Plus DNA synthesizer using solid phase β-cyanoethyl phosphoramidite chemistry at 15 μmol scale. For ODNs with inversion of polarity sites, the synthesis of the 3′-5′ tracts were performed by using normal 3′-phosphoramidites, whereas the 5′-3′ tracts were synthesized by using 5′-phosphoramidites. For all ODNs an universal support was used. The oligomers were detached from the support and deprotected by treatment with concentrated aqueous ammonia at 80°C overnight. The combined filtrates and washings were concentrated under reduced pressure, redissolved in H_2O, analyzed and purified by high-performance liquid chromatography on a Nucleogel SAX column (Macherey-Nagel, 1000-8/46), using buffer A: 20 mM NaH_2PO_4/Na_2HPO_4 aqueous solution (pH 7.0) containing 20% (v/v) CH_3CN and buffer B: 1 M NaCl, 20 mM NaH_2PO_4/Na_2HPO_4 aqueous solution (pH 7.0) containing 20% (v/v) CH_3CN; a linear gradient from 0 to 100% B for 45 min and flow rate 1 ml/min were used. The fractions of the oligomers were collected and successively desalted by Sep-pak cartridges (C-18). The isolated oligomers proved to be >98% pure by NMR.

NMR spectroscopy

NMR samples were prepared at a concentration of ∼1.2 mM, in 0.6 ml (H_2O/D_2O 9:1 v/v) buffer solution having 10 mM KH_2PO_4/K_2HPO_4 or NaH_2PO_4/Na_2HPO_4, 70 mM KCl or NaCl and 0.2 mM EDTA (pH 7.0). Samples purified by HPLC have been desalted, added with the buffer of suitable salt concentration, heated for 5–10 min at 90°C and slowly cooled (10–12 h) to room temperature. The solutions were equilibrated at least for 1 day at 4°C. The folding process was assumed to be complete when ^{1}H NMR spectra were superimposable on changing time. NMR spectra were recorded with Varian Unity INOVA 500 MHz spectrometer. 1D proton spectra of the sample in H_2O were recorded using pulsed-field gradient DPFGSE for H_2O suppression (23). ^{1}H-chemical shifts were referenced relative to external sodium 2,2-dimethyl-2-silapentane-5-sulfonate (DSS). Pulsed-field gradient DPFGSE sequence was used for NOESY (24) (180 and 80 ms mixing times) and TOCSY (25) (120 ms mixing time) experiments in H_2O. All experiments were recorded using STATES-TPPI procedure for quadrature detection (26). In all 2D experiments, the time domain data consisted of 2048 complex points in t2 and 400–512 fids in t1 dimension. A relaxation delay of 1.2 s was used for all experiments.

CD spectroscopy

CD samples of modified oligonucleotides were prepared at an ODN concentration of 50 μM using a potassium phosphate buffer (10 mM KH_2PO_4/K_2HPO_4, 70 mM KCl, pH 7.0) or a sodium phosphate buffer (10 mM NaH_2PO_4/Na_2HPO_4, 70 mM NaCl, pH 7.0) and submitted to the annealing procedure: heating at 90°C and slowly cooling at room temperature. CD spectra of all quadruplexes and CD heating-cooling profiles were registered on a Jasco 715 CD spectrophotometer. For the CD spectra, the wavelength was varied from 220 to 320 nm at 100 nm min^{-1} scan rate, and the spectra recorded with a response of 0.5 s, at 1.0 nm bandwidth and normalized by subtraction of the background scan with buffer. The temperature was kept constant at 5°C with a thermoelectrically-controlled cell holder (Jasco PTC-348). CD heating-cooling profiles were registered as a function of temperature (range: 5–95°C) for all G-quadruplexes at their maximum Cotton effect wavelengths. The CD data were recorded in a 0.1 cm pathlength cuvette with a scan rate of 30°C/h or 10°C/h.

Table 1. Names and sequences of the ODNs investigated

Name	Sequence
mTG_2T	$3'$-$(T_4G_3G_2T_1)_A$-$5'$-$5'$-$(T_1G_2G_3T_4)_B$-$3'$-$3'$-$(T_4G_3G_2T_1)_C$-$5'$-$5'$-$(T_1G_2G_3T_4)_D$-$3'$
mTG_3T	$3'$-$(T_5G_4G_3G_2T_1)_A$-$5'$-$5'$-$(T_1G_2G_3G_4T_5)_B$-$3'$-$3'$-$(T_5G_4G_3G_2T_1)_C$-$5'$-$5'$-$(T_1G_2G_3G_4T_5)_D$-$3'$
mTG_4T	$3'$-$(T_6G_5G_4G_3G_2T_1)_A$-$5'$-$5'$-$(T_1G_2G_3G_4G_5T_6)_B$-$3'$-$3'$-$(T_6G_5G_4G_3G_2T_1)_C$-$5'$-$5'$-$(T_1G_2G_3G_4G_5T_6)_D$-$3'$
$(TG_2T)_4$	$5'$-TGGTTGGTTGGTTGGT-$3'$
$(TG_3T)_4$	$5'$-TGGGTTGGGTTGGGTTGGGT-$3'$
$(TG_4T)_4$	$5'$-TGGGGTTGGGGTTGGGGTTGGGGT-$3'$

Polyacrylamide gel electrophoresis

All ODNs were analyzed by non-denaturing PAGE. Samples in the NMR buffer (10 mM KH_2PO_4/ K_2HPO_4, 70 mM KCl and 0.2 mM EDTA, pH 7) were loaded on a 20% polyacrylamide gel containing Tris–borate-EDTA (TBE) 2.5× and KCl 50 mM. The run buffer was TBE 1× containing 100 mM KCl. For all samples, a solution of glycerol/TBE 1×–100 mM KCl 2:1 was added just before loading. Electrophoresis was performed at 8 V/cm at a temperature close to 10°C. Bands were visualized by UV shadowing.

Cell cultures and treatments with the ODNs

Human p53 mutated lung cancer Calu-6 (ATCC® HTB-56TM) (27), colorectal cancer HCT-116$^{p53-/-}$ (28) and MRC-5 (ATCC® CCL-171) cells were cultured in Dulbecco's Modified Eagle's Medium (DMEM), supplemented with 10% fetal bovine serum (FBS, Euroclone S.p.A.), 2 mM L-glutamine and 50 U/ml penicillin-streptomycin, under humidified atmosphere of 5% CO_2 at 37°C (28). Treatments of cells were performed replacing the culture medium with that containing different ODNs at final concentration of 10 and 50 μM per well from 24 to 72 h (29).

MTT assay

Calu-6 (30), HCT-116 $^{p53-/-}$ and MRC-5 cells were seeded onto 96-well plates at density of 2×10^4 cells/well and treated with different ODNs at final concentration of 10 and 50 μM from 24 to 72 h. Then, cell viability was determined using the MTT assay as previously reported (31). A pool of three different sets of experiments each repeated in triplicate were performed. Error bars represent mean ± SEM from $n = 3$ biological replicates. Statistical comparisons were made as previously shown (32).

Nuclease stability assay

Nuclease stability assay of modified oligonucleotides was conducted in both 10% and 50% FBS diluted with DMEM at 37°C. Approximately 14 nmol of stock solution of each ODN (∼2 O.D.U.) was evaporated to dryness under reduced pressure and then incubated with 500 μl 10% FBS at 37°C. At 0, 24, 48 and 72 h, 125 μl of samples were collected and stored at –20°C for at least 20 min. The samples were evaporated to dryness and then 10 μl of gel loading buffer and 10 μl of autoclaved water was added. 10 μl of the mixture was used for polyacrylamide gel electrophoresis (PAGE), which was carried out at room temperature using 20% polyacrylamide gel in 1× TBE buffer (Tris-borate-EDTA). The degradation patterns on the gel were visualized by UV shadowing.

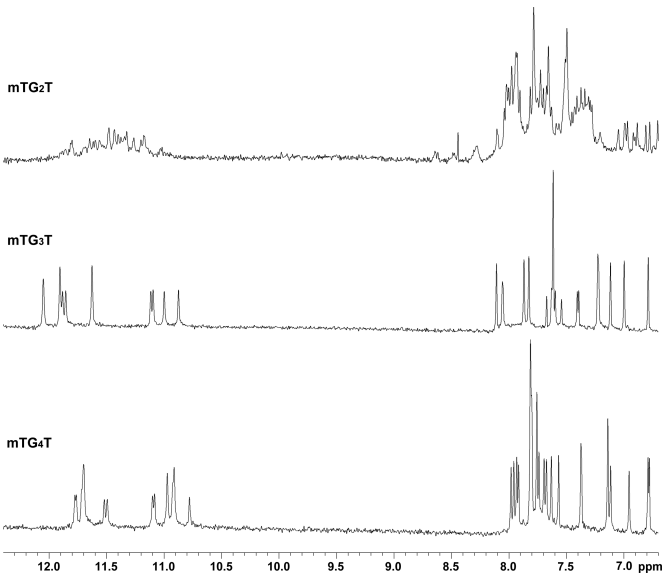

Figure 1. Aromatic and imino proton regions of the ^{1}H NMR spectra (500 MHz) of **mTG_2T**, **mTG_3T** and **mTG_4T** (Table 1) in 10 mM KH_2PO_4/K_2HPO_4, 70 mM KCl and 0.2 mM EDTA (pH 7.0), 25°C.

RESULTS AND DISCUSSION

Nuclear magnetic resonance

In order to verify the ability of ODNs listed in Table 1 to fold in G-quadruplex structures and, in case, to establish their nature, we mainly used NMR experiments. The samples, purified by HPLC, desalted, dried and dissolved in the suitable buffer were heated for 5–10 min at 90°C and slowly cooled down (10–12 h) to room temperature. The solutions were equilibrated at least for one day at 4°C and then their ^{1}H NMR spectra were recorded. The achievement of a completed folding process was guaranteed by the achievement of superimposable ^{1}H NMR spectra on changing time. One of the defining features of structures containing G-tetrads is the appearance of imino proton resonances in the region between 10.5 and 12.0 ppm in NMR spectra (33). Examination of this region is generally used to assess whether the sequence adopts a unique structure. The simple appearance of 1D spectra of **mTG_3T** and **mTG_4T** in potassium buffer (Figure 1 and Supplementary Figure S1) indicates that under the conditions utilized, both the modified oligomers form a mainly single, well-defined hydrogen-bonded conformation consistent with G-quadruplex structures contain-

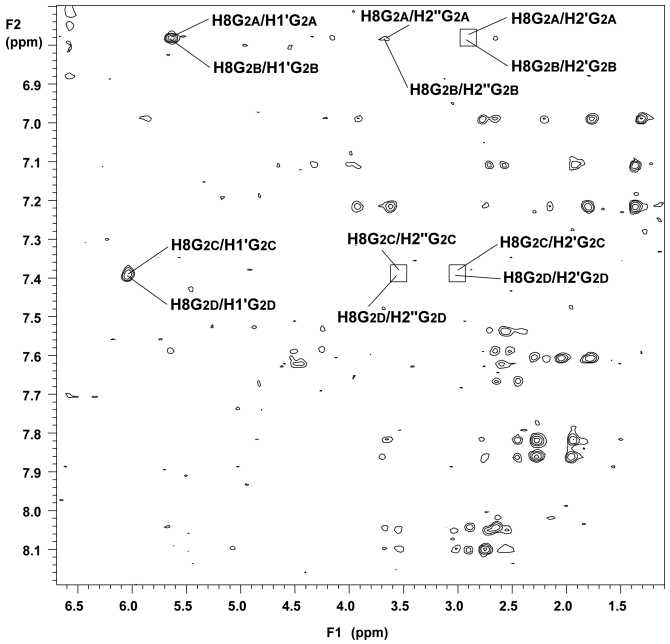

Figure 2. Expanded 2D NOESY spectrum of **mTG$_3$T** (500 MHz; 25°C; strand concentration 1.2 mM; 10 mM KH_2PO_4/K_2HPO_4, 70 mM KCl and 0.2 mM EDTA, pH 7.0 in H_2O/D_2O 9:1; total volume 0.6 ml; mixing time 180 ms) correlating base aromatic protons and sugar protons. Cross-peaks correlating H8G2 and H1′, H2′, H2″ have been highlighted.

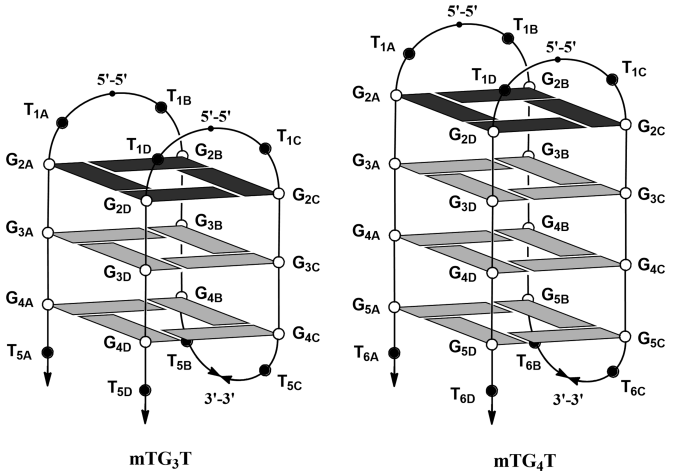

Figure 3. Schematic representation of the G-quadruplex structures adopted by **mTG$_3$T** and **mTG$_4$T** (Table 1). Guanosines in *syn* and *anti* glycosidic conformations are in dark and light gray, respectively. Thymidines are represented by black circles.

ing most likely four and three G-tetrads, respectively. In fact, the ^{1}H NMR spectra of both **mTG$_3$T** and **mTG$_4$T** (500 MHz, $T = 25$°C) showed the presence of twelve and sixteen, partially overlapped signals, respectively, in the region 10.5–12.0 ppm, attributable to imino protons involved in Hoogsteen hydrogen bonds of G-quartets, and of about twenty and twenty-four singlets belonging to guanine H8 and thymine H6 protons in the aromatic region. Furthermore, approximately eight methyl resonances between 1.3 and 2.0 ppm for the eight T-CH_3 were observed for both samples (Supplementary Figure S1). On the other hand, the spectrum of **mTG$_2$T** in potassium buffer at the same temperature came out more complicated than the previous ones. Indeed, in this case, the imino proton region was quite crowded and the number of signals suggested the presence in solution of more than one structure.

In an effort to investigate the main structural features of the G-quadruplex adopted by **mTG$_3$T** and **mTG$_4$T**, we carried out NOESY (Figure 2 and Supplementary Figure S2, respectively) and TOCSY (data not shown) experiments at 25°C. Most of the non-exchangeable protons could be nearly completely assigned following the standard procedures (34) (Supplementary Table S1). As reported for other parallel G-quadruplex structures (35,36), the observed NOEs between G-H8 and T-H6 and their own H1′, H2′ and H2″ protons and the H1′, H2′ and H2″ protons on the 5′-side suggested that both G-quadruplex structures assume a right-handed helical winding. However, some significant differences came out in comparison to the other parallel G-quadruplexes (37): (i) the H8 protons of Gs at the second position displayed unusual upfield chemical shifts if compared to the corresponding protons of the other residues, showing values typical of G-quadruplex structures (38,39); (ii) all the G2 residues adopt *syn* glycosidic angles, as suggested by the comparison between the intense intraresidual H8 e H1′ NOEs and the weak intraresidual H8 and H2′ or H2″ NOEs, whereas the presence of very weak NOEs between G H8/T H6 and H1′ and of strong NOEs between G H8/T H6 and H2′ and H2″ indicated that all the other residues possess an *anti* glycosidic conformation (38–40); (iii) consistently with T(*anti*)-G(*syn*) steps observed for other G-quadruplex structures, the connectivity pattern was broken between residues T1 and G2 (38). Moreover, intrastrand NOEs between the methyl group and H6 protons of T bases and the H8 proton of the G2 ones on the same strand allowed us to assign the T1 residues, suggesting that T residues at the 5′-end are not randomly oriented and are stacked on the plane of the G-tetrads.

Taking into account the relationship between the relative strand orientation and the glycosidic conformation of the guanosines in G-quadruplex structures (41,42), and CD and electrophoretic data suggesting a monomolecular folding (see infra), the collected NMR data would be incompatible with strand arrangements different from the parallel one (Supplementary Figure S3). Therefore, we propose that **mTG$_4$T** and **mTG$_3$T** adopt parallel G-quadruplex structures characterized by one all-*syn* G-tetrad and three or two all-*anti* G-tetrads, respectively, with two T-5′-5′-T and one T-3′-3′-T lateral loops (Figure 3).

The ability of **mTG$_2$T**, **mTG$_3$T** and **mTG$_4$T** to form G-quadruplex structures was further explored in sodium buffer. The appearance of imino proton resonances in the region between 10.5 and 12.0 ppm in the ^{1}H NMR spectrum of **mTG$_4$T** (Supplementary Figure S4) showed that, also in these conditions, this ODN was able to form G-quadruplex structures. However, although the presence of a major conformation could not be ruled out, a substantial peak overlapping prevented us to perform a more detailed NMR analysis. Contrarily to **mTG$_4$T**, the ^{1}H NMR spectrum of **mTG$_3$T** in the same conditions (Supplemen-

tary Figure S4) shows clearly the presence of twelve only partially overlapped signals in the region 10.5–12.0, thus strongly suggesting the presence of a major G-quadruplex conformation. NOESY (Supplementary Figure S5) and TOCSY (data not shown) experiments allowed us to assign most of the non-exchangeable protons following the standard procedures (Supplementary Table S2). In the case of **mTG$_3$T**, the NMR data collected in sodium buffer were very similar to those in potassium buffer previously described, thus confidently suggesting a strict resemblance between the G-quadruplex structures adopted in presence of the two cations. Concerning **mTG$_2$T**, its ^{1}H NMR spectrum showed only a very large low peak in the region 10.5–12.0 and a quite crowed aromatic region, thus indicating the presence of more than one species and a significant amount of random coil.

The NMR data collected for **mTG$_2$T**, **mTG$_3$T** and **mTG$_4$T** were compared to those of their natural versions, namely **(TG$_2$T)$_4$**, **(TG$_3$T)$_4$** and **(TG$_4$T)$_4$**, respectively, both in potassium (Supplementary Figure S6) and sodium buffer (Supplementary Figure S7). Contrarily to **mTG$_2$T**, the ^{1}H NMR spectrum of **(TG$_2$T)$_4$** in potassium buffer did not show imino proton signals in the region 10.5–12.0 ppm, diagnostic for G-quadruplex structures. On the other hand, the ^{1}H NMR spectrum of **(TG$_3$T)$_4$** in the same conditions showed imino proton signals affected by a severe overlapping, while the aromatic proton region appeared quite crowed, thus preventing us to further investigate this ODN. Similarly, although the presence of signals in the imino proton region of the ^{1}H NMR spectrum of **(TG$_4$T)$_4$** would suggest the occurring of G-quadruplex structures also in this case, a poor signal dispersion and a considerable crowing in the aromatic region discouraged us to further study this ODN. Concerning the behavior of **(TG$_2$T)$_4$**, **(TG$_3$T)$_4$** and **(TG$_4$T)$_4$** in sodium buffer, ^{1}H NMR data (Supplementary Figure S7) clearly showed that none of the ODNs is able to form significant amounts of G-quadruplex structures and only the presence of random coil can be supposed.

A straightforward comparison between the NMR data of **mTG$_3$T** and **mTG$_4$T**, from one hand, and **(TG$_3$T)$_4$** and **(TG$_4$T)$_4$** on the other hand, clearly indicates that the presence of inversion of polarity sites, in most of the conditions used, promotes the formation of stable single G-quadruplex structures characterized by well dispersed signals.

CD spectroscopy and thermal denaturation measurements

In investigating G-quadruplex structures, circular dichroism techniques represent an important tool to ascertain the presence of these DNA conformations in solution, obtain preliminary information concerning the structural folding topology or confirm data obtained by different methods, particularly considering that several G-quadruplex types show distinctive CD spectra (43–45). Furthermore, in those cases in which the CD profile is ambiguous, additional topological information could be obtained through a direct comparison between the CD spectrum under investigation and that of specific G-quadruplex structures whose conformation has been ascertained by other techniques.

Figure 4 shows the CD spectra (5°C, 50 μM oligo) of **mTG$_4$T** (A), **mTG$_3$T** (B) and **mTG$_2$T** (C) in different buffer conditions (potassium or sodium phosphate buffer). Both profiles of **mTG$_4$T** and **mTG$_3$T** are characterized by positive bands, differing in intensity, around both 255–260 and 290–295 nm, thus preventing us to assign straightforwardly the CD spectra to a 'Type I' or 'Type II' G-quadruplex CD profile (46). ODN **mTG$_4$T** showed almost superimposable CD profiles in sodium or potassium buffer, thus strongly suggesting that **mTG$_4$T** adopts similar conformations in presence of the two cations. Interestingly, these CD spectra strictly resemble that of a modified TG$_4$T sequence, namely TMGGGT (where M = 8-methyl-2′-deoxyguanosine), which was proven by NMR to form a tetramolecular parallel G-quadruplex with three G-tetrads all-*anti* and one M-tetrad all-*syn* at the 5′-end (Figure 4A) (47). Taking into account that generally the occurrence of a maximum around 290–295 nm is indicative of the presence of G-residues adopting *syn* glycosidic conformations (43), these data suggest that **mTG$_4$T** folds in a G-quadruplex structure characterized by the same strands orientation and tetrads arrangements of the tetramolecular G-quadruplex formed by TMGGGT, in agreement with the strand orientation of the G-quadruplex structure inferred by NMR data (Figure 3). Similarly, apart from differences in band intensities with the potassium buffer profile, probably due to the better ability of potassium than sodium ions to stabilize G-quadruplex conformations, and slight differences in wavelengths, **mTG$_3$T** showed CD spectra similar to that of the tetramolecular G-quadruplex formed by TMGGT (Figure 4B) which, according to NMR investigations, is characterized by two G-tetrads all-*anti* and one M-tetrad all-*syn* at the 5′-end (48). Thus, similarly to **mTG$_4$T** and in agreement with NMR data, CD data suggested that **mTG$_3$T** adopts a G-quadruplex structure characterized by the same strands orientation and tetrads arrangements of the tetramolecular G-quadruplex formed by TMGGT. As far **mTG$_2$T** is concerned, the CD spectrum in potassium buffer showed a 'Type II' profile with two positive bands at 252 and 297 nm and one negative band at 272 nm. On the other hand, the CD profile in sodium buffer could be defined as 'Type I', apart from a minor positive band at 296 nm. Taking into account the relationship between CD spectrum and G-tetrad stacking (43), several G-quadruplex topologies would be compatible with the CD profiles observed (see some examples in Supplementary Figure S8), in agreement with NMR spectra suggesting the presence of more than one conformation in this case.

CD was also used to evaluate the thermal stability both in sodium and potassium buffer of the G-quadruplex structures investigated. CD melting profiles of all the ODNs containing IPSs are shown in Supplementary Figure S9. CD heating curves of **mTG$_4$T**, both in presence of potassium (datum not shown) and sodium ions (70 mM, Supplementary Figure S9A), showed no sigmoidal profiles but only a slightly diminished CD signal at 90°C. In an attempt to obtain suitable melting profiles, CD heating curves were recorded also in presence of 5 mM potassium or sodium ions (Supplementary Figure S9B). Also in these cases no sigmoidal profiles were achieved but only a decrease of CD signals at 95°C was observed. These data clearly demonstrate that G-quadruplex **mTG$_4$T** is endowed with an extraordinary thermal stability, in agreement with the paral-

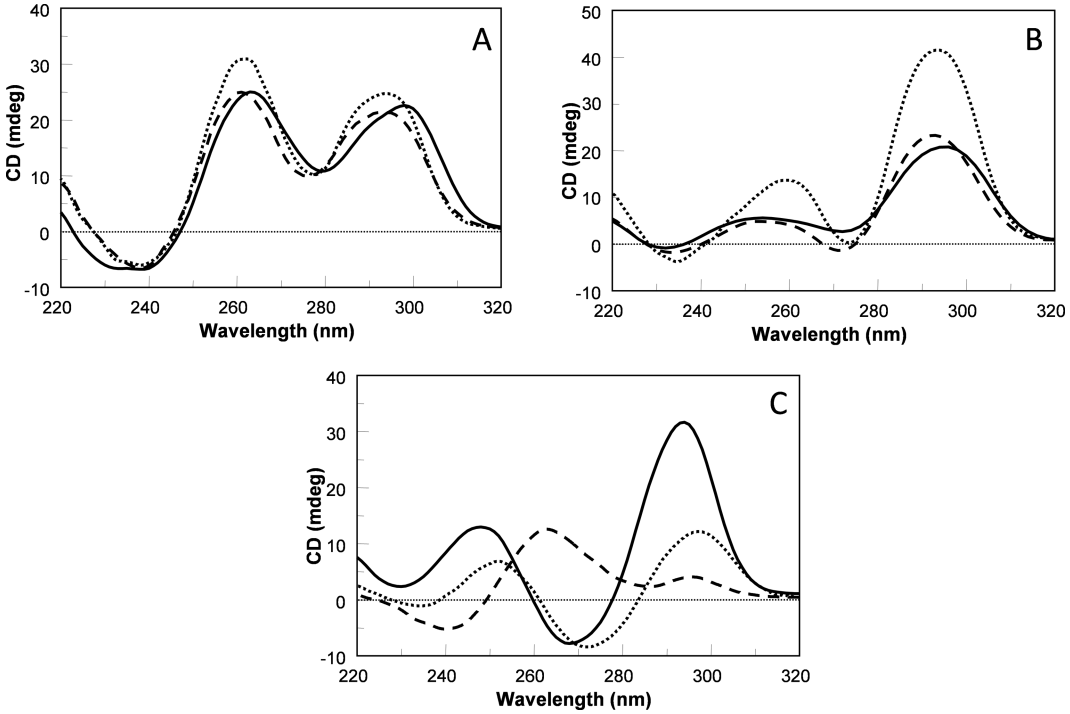

Figure 4. CD spectra at 5°C of (**A**) **mTG$_4$T** in potassium (. . .) and sodium buffer (|), compared to TMGGGT complex (---); (**B**) **mTG$_3$T** in potassium (. . .) and sodium buffer (|), compared to TMGGT complex (---); (**C**) **mTG$_2$T** in potassium (. . .) and sodium buffer (|) compared to TBA (---).

lel strand arrangement suggested by NMR and CD data. In order to obtain preliminary data about the molecularity of the G-quadruplex formed by **mTG$_4$T**, CD spectra at decreasing concentrations of ODN were recorded, as reported by other authors (46) (Supplementary Figure S10A). The independence of the CD profile on strand concentration is in good agreement with the presence of a monomolecular structure. A further datum supporting the occurring of a monomolecular structure is the linear dependence of the CD signal intensity (both at 262 and 294 nm) on the strand concentration (Supplementary Figure S10B and C).

The CD heating curve of **mTG$_3$T** in potassium buffer only showed a decreased CD signal at 95°C, thus indicating an outstanding thermal stability also in this case. However, the CD heating curve of **mTG$_3$T** in sodium buffer was characterized by a well-defined sigmoidal profile that allowed us to measure the melting temperature (T_m) in these conditions (75°C) (Supplementary Figure S9C and D). The absence of hysteresis between heating and cooling profiles is in agreement with the occurring of a monomolecular G-quadruplex structure also in this case (Supplementary Figure S9D). Contrarily to the previous cases, CD melting profile of **mTG$_2$T** in potassium buffer was sigmoidal, thus affording a T_m of 40°C, in agreement with a G-quadruplex structure formed by only two stacked G-tetrads. However, the evident hysteresis between heating-cooling curves suggests the simultaneous presence of structures with different stabilities and folding rates, as already suggested by NMR data. On the other hand, the CD heating-cooling curves of **mTG$_2$T** in sodium buffer did not show a good sigmoidal profile, probably due to its quite low thermal stability (Supplementary Figure S9E and F).

Since ^{1}H NMR spectra of **(TG$_3$T)$_4$** and **(TG$_4$T)$_4$** in potassium buffer suggested the presence of G-quadruplex structures, also their CD spectra and heating profiles were recorded in a buffer 10 mM KH_2PO_4/K_2HPO_4, 70 mM KCl, pH 7.0 (Supplementary Figure S11). The CD spectrum of **(TG$_4$T)$_4$**, showing a negative band at 236 nm and two positive bands at 266 and 294 nm, resembles that of **mTG$_4$T**, thus suggesting a similar G-tetrad stacking. However, the band intensity of **(TG$_4$T)$_4$** was quite low respect to **mTG$_4$T**. On the contrary, the CD profile of **(TG$_3$T)$_4$** was quite different from that of **mTG$_3$T**, since it showed a negative and a positive band at 242 and 264 nm, respectively, being indicative of a parallel G-quadruplex structure with all guanosines adopting *anti* glycosidic conformations. CD heating profile of **(TG$_4$T)$_4$** indicated a melting temperature of 83°C. Then, thermal stability of **(TG$_4$T)$_4$** is definitely lower than **mTG$_4$T**, for which a melting temperature higher than 95°C was indicated by its CD heating profile acquired even at a much lower potassium concentration (Supplementary Figure S9B). Similarly, although CD heating curve of **(TG$_3$T)$_4$** did not show a sigmoidal profile, it suggested a thermal stability definitively lower than **mTG$_3$T**, considering that its CD heating curve indicated a melting temperature higher than 95°C in the same conditions (Supplementary Figure S9C).

Using NMR results and according to CD data, we built approximate molecular models of both quadruplexes formed by **mTG$_3$T** and **mTG$_4$T**, as described in the Supplementary Data (Supplementary Figure S12), with the aim to verify the compatibility of the TT loops containing inversion of polarity sites with the parallel arrangement of the

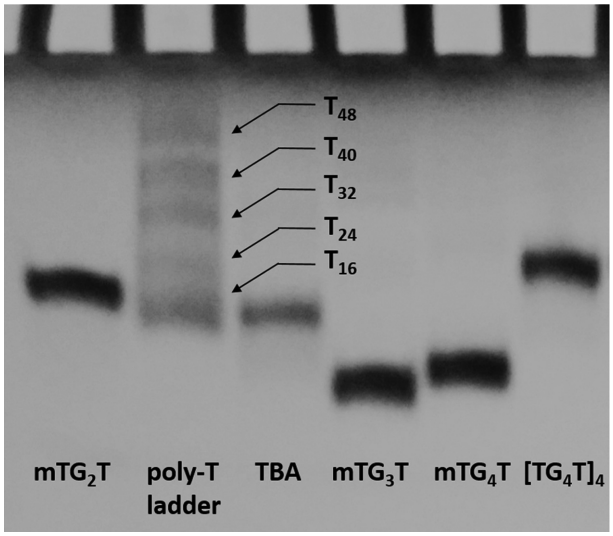

Figure 5. Polyacrylamide gel electrophoresis of the ODNs with inversion of polarity sites investigated (Table 1). A ladder of poly-T ODNs, TBA ($G_2T_2G_2TGTG_2T_2G_2$) and the tetramolecular parallel G-quadruplex structure formed by TG_4T have been used as references.

strands and verify the presence of possible backbone distortions.

Polyacrylamide gel electrophoresis

In order to acquire additional insight about the molecularity of the G-quadruplex structures investigated, all ODNs containing IPSs were further analyzed by PAGE and compared with a poly-T ladder, TBA and tetramolecular TG_4T, used as references (Figure 5). Concerning **mTG$_3$T** and **mTG$_4$T**, the electrophoretic profile shows that they were characterized by single well-defined bands with a rather faster mobility than T_{16} and T_{24}, thus suggesting the presence of major monomolecular structures. As expected, **mTG$_3$T** and **mTG$_4$T** migrated faster than the tetramolecular G-quadruplex $[TG_4T]_4$, taking into account their higher charge to mass ratios, due to the additional three IPS phosphate groups. As far as **mTG$_2$T** is concerned, the ODN sample showed a major band with a motility similar to that of TBA, although it migrated slightly slower. Taking into account the very similar charge to mass ratios of TBA and **mTG$_2$T**, this datum suggests that, also in this case, monomolecular G-quadruplex structures occur. On the other hand, the slightly slower mobility of **mTG$_2$T** compared to TBA, could be tentatively explained by the presence of G-quadruplex structures with three propeller loops (Supplementary Figure S8), in which the G-tetrad arrangement is compatible with the CD profiles. It should be noted that in no case higher order structures could be observed.

Antiproliferative activity

In order to study the antiproliferative activities of the investigated ODNs, MTT assays were performed in Calu-6 and HCT-116$^{p53-/-}$ cells treated with two concentrations of ODNs, 10 and 50 μM, for 24, 48 and 72 h. As a result, all tested ODNs consistently inhibited proliferation in these tumor cell lines in time and dose dependent manner. In particular, in Calu-6 cell line, among the tested ODNs, **mTG$_4$T** showed the highest activity at both tested concentrations. Specifically, **mTG$_4$T** showed the 50% of its antiproliferative activity at 50 μM after 24 h of incubation while for the other ODNs the same antiproliferative activity was obtained after 36 h (**mTG$_3$T,** and **mTG$_2$T** in potassium buffer) or 48 h (**mTG$_2$T** in sodium buffer) of incubation (Figure 6 and Supplementary Figure S13). However, all tested ODNs reduced the cell viability of Calu-6 cells of ∼80% after 72 h of treatment. Similar results have been observed on HCT-116$^{p53-/-}$ cells (Supplementary Figure S14). In contrast to tumor cell line, MRC-5 cells which are derived from normal lung fibroblasts were found to be considerably less sensitive to the antiproliferative effects of all tested ODNs (Supplementary Figure S15). The antiproliferative activity on Calu-6 cells was evaluated also for natural ODNs **(TG$_2$T)$_4$**, **(TG$_3$T)$_4$** and **(TG$_4$T)$_4$** (Supplementary Figure S16). All natural ODNs were able to inhibit proliferation until 48 h. In particular, the activity trend at 50 μM was **(TG$_2$T)$_4$** > **(TG$_3$T)$_4$** > **(TG$_4$T)$_4$**. However, in these cases, a dramatic decrease of the cytotoxicity after 72 h of incubation at both ODN concentrations was clearly evident, in strong contrast with ODNs containing IPS for which a remarkable antiproliferative activity was observed after the same incubation time. The observed data could be explained taking into account the contribution of guanine-based degradation products; this effect has been recently described (49). This hypothesis is in agreement with the trend of degradability observed in the FBS assay (see infra) in which **(TG$_4$T)$_4$** and **(TG$_2$T)$_4$** were the most and the least resistant ones, respectively. Therefore, the temporary antiproliferative activity observed for natural ODNs should be considered non-specific and then, involving no particular protein target. The observed cell specificity for cancer cells of ODNs containing IPS tested together with their ability to exert antiproliferative activity on cultured cells in the absence of transfection agent suggest a mechanism of internalization mediated by an oligonucleotide receptor, not yet identified, more expressed in cancer cells than in normal cells as already demonstrated for other G-rich oligonucleotides (50). Further studies are required to investigate the mechanism underlying the growth inhibitory effects of tested ODNs containing IPSs.

Nuclease stability assay

Since all ODNs investigated have shown noteworthy antiproliferative activities, their resistance in biological environments was evaluated through a degradation assay in both 10% and 50% FBS followed by gel electrophoresis analysis, in view of a potential development as therapeutic agents. Considering that the cell viability measured by the MTT assays was tested up to 72 h, the resistance of the ODNs was evaluated after 24, 48 and 72 h. The electrophoretic profiles showed clearly that, in 10% FBS, **mTG$_3$T** was partially resistant after 72 h, while **mTG$_4$T** was completely resistant after the same time (Figure 7), despite the fact that they are characterized by two 3′-ends, particularly susceptible to the more abundant 3′-exonucleases. Probably, the reasons for this resistance are that the G-

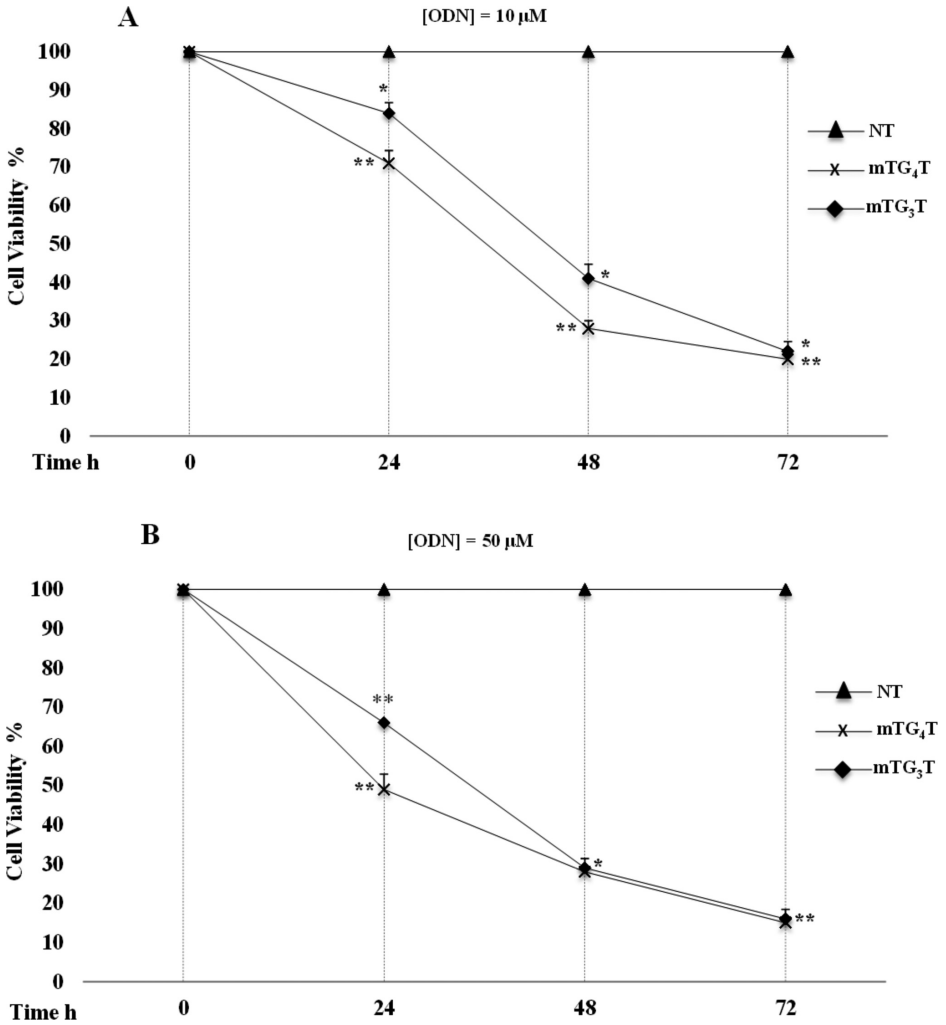

Figure 6. Antiproliferative activity of ODNs **mTG$_3$T** and **mTG$_4$T** on Calu-6 cell line. Cells were treated with two different concentrations of ODNs, 10 μM (**A**) and 50 μM (**B**), from 24 to 72 h. The line NT (not treated) reports the cell viability in absence of ODNs. Cell viability was assayed using the MTT assay. Results are presented as percentage (mean ± SEM) ($n = 3$) of the control cells. *$P < 0.05$, **$P < 0.01$.

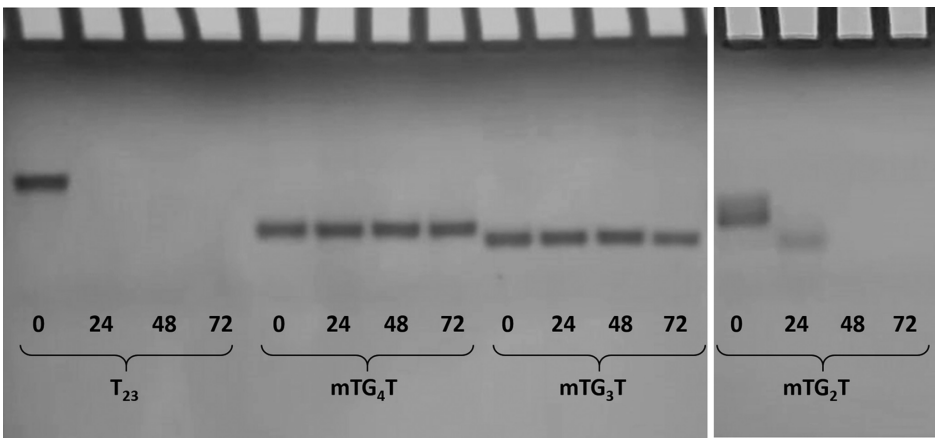

Figure 7. Stability of the IPS-containing ODNs investigated in 10% fetal bovine serum (FBS) at 0, 24, 48 and 72 h, as monitored by non-denaturing PAGE. ODN T_{23} has been used as positive control. See the Materials and Methods section for experimental details.

quadruplex structures formed by **mTG$_3$T** and **mTG$_4$T** are not good substrates for the exonucleases and the amount of random coil in equilibrium with the folded specie can be considered negligible, due to their exceptional thermal stability. G-quadruplex structures **mTG$_3$T** and **mTG$_4$T** showed a certain resistance also in 50% FBS, although a decrease of the band intensities after 72 h indicated minor amounts of unaffected structure, as expected (Supplementary Figure S17). On the other hand, **mTG$_2$T** was mostly degraded in 10% FBS after 24 h (Figure 7) or completely degraded (in 50% FBS) after 72 h (Supplementary Figure S17). This datum is not surprising, taking into account the temperature used during the assay and the relatively low thermal stability observed for structures formed by **mTG$_2$T**, that imply the presence of a significant amount of degradable random coil.

A similar 10% FBS degradation assay was also used to evaluate the resistance to nucleases of the natural ODNs after 24, 48 and 72 h (Supplementary Figure S18). The electrophoretic profile suggests the following trend of decreasing degradation: **(TG$_2$T)$_4$** > **(TG$_3$T)$_4$** > **(TG$_4$T)$_4$**. This result is in agreement with data obtained by NMR and CD experiments indicating no G-quadruplex formation for **(TG$_2$T)$_4$**, G-quadruplex structures characterized by a low thermal stability for **(TG$_3$T)$_4$** and quite stable G-quadruplex structures for **(TG$_4$T)$_4$**.

CONCLUSIONS

One of the most important reasons for the great spread of G-quadruplex structures and their occurring in several research fields and large applicability in technology is their extreme structural variability. Apart from by changing the base-sequence and experimental conditions, this variability can be expanded also through suitable chemical modifications. In an effort to exploit the potential of the IPSs to spread out the topological repertoire of the G-quadruplex structures, we have designed and investigated three sequences containing both 3′-3′ and 5′-5′ IPSs, characterized by four G-runs with two, three and four residues. In the cases of **mTG$_3$T** and **mTG$_4$T**, CD, NMR and electrophoresis data suggested that they fold in extraordinarily stable monomolecular parallel G-quadruplex structures characterized by one all-*syn* G-tetrad at the 5′-end, two (**mTG$_3$T**) or three (**mTG$_4$T**) all-*anti* G-tetrads and three TT lateral loops containing one 3′-3′ and two 5′-5′ IPSs. Although these peculiar strand and G-tetrad stacking arrangements are rather uncommon, they have been already found in both natural and modified G-quadruplex forming sequences. For example, the G-rich sequence of the oncogene RET promoter forms a monomolecular parallel G-quadruplex structure with a G-tetrad arrangement similar to **mTG$_3$T**, characterized by three double-chain reversal loops (51) Remarkably, ODN TG$_3$T, beside adopting a tetramolecular parallel G-quadruplex with all-*anti* G-tetrads, it forms also a tetramolecular parallel G-quadruplex with an all-*syn* and two all-*anti* G-tetrads as a minor specie. On the other hand, also suitably modified ODNs containing a 5′-5′ IPS adjacent to the G-run (namely, ODN 3′-T-5′-5′-GGGT-3′) or 8-Br (52) or 8-methyl-2'-deoxyguanosines, all promoting the glycosidic *syn* conformation, are able to adopt stable G-tetrad arrangements similar to **mTG$_3$T** and **mTG$_4$T**. It should be noted that natural sequences similar to **mTG$_2$T**, **mTG$_3$T** and **mTG$_4$T** but lacking of IPSs, namely **(TG$_2$T)$_4$**, **(TG$_3$T)$_4$**and **(TG$_2$T)$_4$**, respectively, in the same conditions, were not able to form G-quadruplex structures or single structures characterized by simple ^{1}H NMR spectra.

All ODNs here investigated have shown an interesting anti-proliferative activity against cancer lung cells (Calu-6) and colorectal cancer cells (HCT-116$^{p53-/-}$), while no effects on normal lung fibroblasts have been observed. Taking into account the excellent resistance of **mTG$_3$T** and **mTG$_4$T** to degradation in fetal bovine serum, their biological activity cannot be ascribed to the cytotoxicity of guanine-based degradation products that has been recently described (49). These considerations suggest that the antiproliferative activity of **mTG$_3$T** and **mTG$_4$T** could depend on specific biological pathways and targets. Several investigations have reported that nucleolin is the main target involved in the ascertained antiproliferative activity of various G-rich ODNs (53–55). Very recently, by evaluating the binding ability to nucleolin of several G-quadruplex forming ODNs, Lago et al. have suggested that this cellular protein preferentially binds long-looped G-quadruplex structures (56). Then, although it could not completely ruled out, it is improbable that nucleolin could be involved in the antiproliferative activity of **mTG$_3$T** and **mTG$_4$T** since our investigations pointed to G-quadruplex structures devoid of long loops. These data strongly suggest the involvement of biological pathways not yet taken into consideration; experiments in this frame have be planned in our laboratories aimed at identifying a probable new protein target.

An interesting structural feature, present in parallel **mTG$_3$T** and **mTG$_4$T** G-quadruplexes but lacking in unmodified monomolecular parallel G-quadruplexes, is the occurring of both the ODN ends on the same side of the structure. This structural characteristic is fundamental in designing analytical molecular devices by the FRET approach in which donor and quencher molecules are linked to the ODN ends (57). Then, the propensity of parallel G-quadruplex structures to interact with heavy metal cations (58) and the dependence of their formation and stability on K^+ could be exploited in designing more efficient analytical molecular systems for the detection of these ions (59).

A further possible application of the monomolecular parallel G-quadruplexes containing IPSs here proposed concerns their potential as anti-HIV aptamers. In fact, two tetramolecular parallel G-quadruplex aptamers have been described in literature, namely the Hotoda's aptamer (60,61) and ISIS5320 (62) which have both suggested to interact with the HIV glycoprotein 120. However, their development has been limited by their quite low formation rates (63). This drawback could be circumvented by designing parallel G-quadruplexes containing IPSs with the suitable sequences, which, thanks to their monomolecular nature, would be characterized by higher formation rate and stabilities, besides preserving the main features of the original parallel G-quadruplex structures. A similar approach has been successful applied in the monomolecular tetra-end-linked (TEL-ODNs) version of the Hotoda's aptamer (64,65).

SUPPLEMENTARY DATA

Supplementary Data are available at NAR Online.

FUNDING

Regione Campania under POR Campania [FESR 2007–2013-O.O. 2.1] (FarmaBioNet). Funding for open access charge: Dipartimento di Farmacia, Università di Napoli Federico II.
Conflict of interest statement. None declared.

REFERENCES

1. Maizels,N. and Gray,L.T. (2013) The G4 Genome. *PLoS Genet.*, **9**, e1003468.
2. Siddiqui-Jain,A., Grand,C.L., Bearss,D.J. and Hurley,L.H. (2002) Direct evidence for a G-quadruplex in a promoter region and its targeting with a small molecule to repress c-MYC transcription. *Proc. Natl. Acad. Sci. U.S.A.*, **99**, 11593–11598.
3. Kumari,S., Bugaut,A., Huppert,J.L. and Balasubramanian,S. (2007) An RNA G-quadruplex in the 5′ UTR of the NRAS proto-oncogene modulates translation. *Nat. Chem. Biol.*, **3**, 218–221.
4. Cahoon,L.A. and Seifert,H.S. (2009) An alternative DNA structure is necessary for pilin antigenic variation in Neisseria gonorrhoeae. *Science*, **325**, 764–767.
5. Cogoi,S. and Xodo,L.E. (2006) G-quadruplex formation within the promoter of the KRAS proto-oncogene and its effect on transcription. *Nucleic Acids Res.*, **34**, 2536–2549.
6. Paeschke,K., Capra,J.A. and Zakian,V.A. (2011) DNA replication through G-quadruplex motifs is promoted by the Saccharomyces cerevisiae Pif1 DNA helicase. *Cell*, **145**, 678–691.
7. Bugaut,A. and Balasubramanian,S. (2012) 5′-UTR RNA G-quadruplexes: translation regulation and targeting. *Nucleic Acids Res.*, **40**, 4727–4741.
8. Sun,D., Guo,K., Rusche,J.J. and Hurley,L.H. (2005) Facilitation of a structural transition in the polypurine/polypyrimidine tract within the proximal promoter region of the human VEGF gene by the presence of potassium and G-quadruplex-interactive agents. *Nucleic Acids Res.*, **33**, 6070–6080.
9. Varizhuk,A., Ilyinsky,N., Smirnov,I. and Pozmogova,G. (2016) G4 aptamers: trends in structural design. *Mini-Rev. Med. Chem.*, **16**, 1321–1329.
10. Tucker,W.O., Shum,K.T. and Tanner,J.A. (2012) G-quadruplex DNA aptamers and their ligands: structure, function and application. *Curr. Pharm. Des.*, **18**, 2014–2026.
11. Yatsunyk,L.A., Mendoza,O. and Mergny,J.L. (2014) 'Nano-oddities': Unusual nucleic acid assemblies for DNA-based nanostructures and nanodevices. *Acc. Chem. Res.*, **47**, 1836–1844.
12. Sagi,J. (2014) G-quadruplexes incorporating modified constituents: a review. *J. Biomol. Struct. Dyn.*, **32**, 477–511.
13. Galeone,A., Mayol,L., Virgilio,A., Virno,A. and Randazzo,A. (2008) A further contribution to the extreme variability of quadruplex structures from oligodeoxyribonucleotides containing inversion of polarity sites in the G-tract. *Mol. Biosyst.*, **4**, 426–430.
14. Esposito,V., Virgilio,A., Pepe,A., Oliviero,G., Mayol,L. and Galeone,A. (2009) Effects of the introduction of inversion of polarity sites in the quadruplex forming oligonucleotide TGGGT. *Bioorg. Med. Chem.*, **17**, 1997–2001.
15. Virgilio,A., Esposito,V., Mangoni,A., Mayol,L. and Galeone,A. (2013) A novel equilibrium relating to the helix handedness in G-quadruplexes formed by heterochiral oligonucleotides with an inversion of polarity site. *Chem. Commun. (Camb).*, **49**, 7935–7937.
16. Esposito,V., Galeone,A., Mayol,L., Randazzo,A., Virgilio,A. and Virno,A. (2007) A mini-library of TBA analogues containing 3′-3′ and 5′-5′ inversion of polarity sites. *Nucleosides Nucleotides Nucleic Acids*, **26**, 1145–1159.
17. Esposito,V., Scuotto,M., Capuozzo,A., Santamaria,R., Varra,M., Mayol,L., Virgilio,A. and Galeone,A. (2014) A straightforward modification in the thrombin binding aptamer improving the stability, affinity to thrombin and nuclease resistance. *Org. Biomol. Chem.*, **12**, 8840–8843.
18. Virgilio,A., Amato,T., Petraccone,L., Filosa,R., Varra,M., Mayol,L., Esposito,V. and Galeone,A. (2016) Improved thrombin binding aptamer analogues containing inversion of polarity sites: Structural effects of extra-residues at the ends. *Org. Biomol. Chem.*, **14**, 7707–7714.
19. Esposito,V., Russo,A., Amato,T., Varra,M., Vellecco,V., Bucci,M., Russo,G., Virgilio,A. and Galeone,A. (2017) Backbone modified TBA analogues endowed with antiproliferative activity. *Biochim. Biophys. Acta - Gen. Subj.*, **1861**, 1213–1221.
20. Jin,R., Gaffney,B.L., Wang,C., Jones,R.a and Breslauer,K.J. (1992) Thermodynamics and structure of a DNA tetraplex: a spectroscopic and calorimetric study of the tetramolecular complexes of d(TG_3T) and d($TG_3T_2G_3T$). *Proc. Natl. Acad. Sci. U.S.A.*, **89**, 8832–8836.
21. Aboul-ela,F., Murchie,A.I.H. and Lilley,D.M. (1992) NMR study of parallel-stranded tetraplex formation by the hexadeoxynucleotide d(TG_4T). *Nature*, **360**, 280–282.
22. Do,N.Q., Lim,K.W., Teo,M.H., Heddi,B. and Phan,A.T. (2011) Stacking of G-quadruplexes: NMR structure of a G-rich oligonucleotide with potential anti-HIV and anticancer activity. *Nucleic Acids Res.*, **39**, 9448–9457.
23. Dalvit,C. (1998) Efficient multiple-solvent suppression for the study of the interactions of organic solvents with biomolecules. *J. Biomol. NMR*, **11**, 437–444.
24. Jeener,J., Meier,B.H., Bachmann,P. and Ernst,R.R. (1979) Investigation of exchange processes by two-dimensional NMR spectroscopy. *J. Chem. Phys.*, **71**, 4546.4553
25. Braunschweiler,L. and Ernst,R.R. (1983) Coherence transfer by isotropic mixing: application to proton correlation spectroscopy. *J. Magn. Reson.*, **53**, 521–528.
26. Marion,D., Ikura,M., Tschudin,R. and Bax,A. (1989) Rapid recording of 2D NMR spectra without phase cycling. Application to the study of hydrogen exchange in proteins. *J. Magn. Reson.*, **85**, 393–399.
27. Bunz,F., Dutriaux,A., Lengauer,C., Waldman,T., Zhou,S., Brown,J.P., Sedivy,J.M., Kinzler,K.W. and Vogelstein,B. (1998) Requirement for p53 and p21 to sustain G2 arrest after DNA damage. *Science*, **282**, 1497–1501.
28. Esposito,D., Crescenzi,E., Sagar,V., Loreni,F., Russo,A. and Russo,G. (2014) Human rpL3 plays a crucial role in cell response to nucleolar stress induced by 5-FU and L-OHP. *Oncotarget*, **5**, 11737–11751.
29. Di Villa Bianca,R.D. emmanuele, Mitidieri,E., Esposito,D., Donnarumm,E., Russo,A., Fusco,F., Ianaro,A., Mirone,V., Cirino,G., Russo,G. *et al.* (2015) Human cystathionine-β-synthase phosphorylation on serine227 modulates hydrogen sulfide production in human urothelium. *PLoS One*, **10**, 1–16.
30. Russo,A., Pagliara,V., Albano,F., Esposito,D., Sagar,V., Loreni,F., Irace,C., Santamaria,R. and Russo,G. (2016) Regulatory role of rpL3 in cell response to nucleolar stress induced by act D in tumor cells lacking functional p53. *Cell Cycle*, **15**, 41–51.
31. Maiolino,S., Russo,A., Pagliara,V., Conte,C., Ungaro,F., Russo,G. and Quaglia,F. (2015) Biodegradable nanoparticles sequentially decorated with Polyethyleneimine and Hyaluronan for the targeted delivery of docetaxel to airway cancer cells. *J. Nanobiotechnology*, **13**, 29.
32. De Filippis,D., Russo,A., De Stefano,D., Cipriano,M., Esposito,D., Grassia,G., Carnuccio,R., Russo,G. and Iuvone,T. (2014) Palmitoylethanolamide inhibits rMCP-5 expression by regulating MITF activation in rat chronic granulomatous inflammation. *Eur. J. Pharmacol.*, **725**, 64–69.
33. Feigon,J., Koshlap,K.M. and Smith,F.W. (1995) ^{1}H NMR spectroscopy of DNA triplexes and quadruplexes. *Methods Enzymol.*, **261**, 225–255.
34. Wüthrich,K. (1986) *NMR of Proteins and Nucleic Acids* John Wiley and Sons, NY.
35. Patel,P.K., Bhavesh,N.S. and Hosur,R. V (2000) Cation-dependent conformational switches in d-TGGCGGC containing two triplet repeats of Fragile X Syndrome: NMR observations. *Biochem. Biophys. Res. Commun.*, **278**, 833–838.
36. Patel,P.K. and Hosur,R. V. (1999) NMR observation of T-tetrads in a parallel stranded DNA quadruplex formed by Saccharomyces cerevisiae telomere repeats. *Nucleic Acids Res.*, **27**, 2457–2464.
37. Aboul-ela,F., Murchie,A.I.H., Norman,D.G. and Lilley,D.M.J. (1994) Solution structure of a parallel-stranded tetraplex formed by

d(TG_4T) in the presence of sodium ions by nuclear magnetic resonance spectroscopy. *J. Mol. Biol.*, **243**, 458–471.
38. Smith,F.W. and Feigon,J. (1993) Strand orientation in the DNA quadruplex formed from the Oxytricha telomere repeat oligonucleotide d($G_4T_4G_4$) in solution. *Biochemistry*, **32**, 8682–8692.
39. Yu Wang,K., McCurdy,S., Shea,R.G., Swaminathan,S. and Bolton,P.H. (1993) A DNA Aptamer Which Binds to and Inhibits Thrombin Exhibits a New Structural Motif for DNA. *Biochemistry*, **32**, 1899–1904.
40. Virgilio,A., Esposito,V., Randazzo,A., Mayol,L. and Galeone,A. (2005) Effects of 8-methyl-2'-deoxyadenosine incorporation into quadruplex forming oligodeoxyribonucleotides. *Bioorganic Med. Chem.*, **13**, 1037–1044.
41. Karsisiotis,A.I., O'Kane,C. and Webba da Silva,M. (2013) DNA quadruplex folding formalism—a tutorial on quadruplex topologies. *Methods*, **64**, 28–35.
42. Esposito,V., Galeone,A., Mayol,L., Oliviero,G., Virgilio,A. and Randazzo,L. (2007) A topological classification of G-quadruplex structures. *Nucleosides, Nucleotides Nucleic Acids*, **26**, 1155–1159.
43. Masiero,S., Trotta,R., Pieraccini,S., De Tito,S., Perone,R., Randazzo,A. and Spada,G.P. (2010) A non-empirical chromophoric interpretation of CD spectra of DNA G-quadruplex structures. *Org. Biomol. Chem.*, **8**, 2683–2692.
44. Vorlíčková,M., Kejnovská,I., Sagi,J., Renčiuk,D., Bednářová,K., Motlová,J. and Kypr,J. (2012) Circular dichroism and guanine quadruplexes. *Methods*, **57**, 64–75.
45. Kypr,J., Kejnovská,I., Renčiuk,D. and Vorlíčková,M. (2009) Circular dichroism and conformational polymorphism of DNA. *Nucleic Acids Res.*, **37**, 1713–1725.
46. Tran,P.L.T., Mergny,J.L. and Alberti,P. (2011) Stability of telomeric G-quadruplexes. *Nucleic Acids Res.*, **39**, 3282–3294.
47. Thao Tran,P.L., Virgilio,A., Esposito,V., Citarella,G., Mergny,J.L. and Galeone,A. (2011) Effects of 8-methylguanine on structure, stability and kinetics of formation of tetramolecular quadruplexes. *Biochimie*, **93**, 399–408.
48. Virgilio,A., Esposito,V., Randazzo,A., Mayol,L. and Galeone,A. (2005) 8-Methyl-2'-deoxyguanosine incorporation into parallel DNA quadruplex structures. *Nucleic Acids Res.*, **33**, 6188–6195.
49. Zhang,N., Bing,T., Liu,X., Qi,C., Shen,L., Wang,L. and Shangguan,D. (2015) Cytotoxicity of guanine-based degradation products contributes to the antiproliferative activity of guanine-rich oligonucleotides. *Chem. Sci.*, **6**, 3831–3838.
50. Bates,P.J., Laber,D.A., Miller,D.M., Thomas,S.D. and Trent,J.O. (2009) Discovery and development of the G-rich oligonucleotide AS1411 as a novel treatment for cancer. *Exp. Mol. Pathol.*, **86**, 151–164.
51. Tong,X., Lan,W., Zhang,X., Wu,H., Liu,M. and Cao,C. (2011) Solution structure of all parallel G-quadruplex formed by the oncogene RET promoter sequence. *Nucleic Acids Res.*, **39**, 6753–6763.
52. Karg,B., Haase,L., Funke,A., Dickerhoff,J. and Weisz,K. (2016) Observation of a dynamic G-tetrad flip in intramolecular G-quadruplexes. *Biochemistry*, **55**, 6949–6955.
53. Bates,P.J., Kahlon,J.B., Thomas,S.D., Trent,J.O. and Miller,D.M. (1999) Antiproliferative activity of G-rich oligonucleotides correlates with protein binding. *J. Biol. Chem.*, **274**, 26369–26377.
54. Girvan,A.C., Teng,Y., Casson,L.K., Thomas,S.D., Jüliger,S., Ball,M.W., Klein,J.B., Pierce,W.M., Barve,S.S. and Bates,P.J. (2006) AGRO100 inhibits activation of nuclear factor-kappaB (NF-kappaB) by forming a complex with NF-kappaB essential modulator (NEMO) and nucleolin. *Mol. Cancer Ther.*, **5**, 1790–1799.
55. Teng,Y., Girvan,A.C., Casson,L.K., Pierce,W.M., Qian,M., Thomas,S.D. and Bates,P.J. (2007) AS1411 alters the localization of a complex containing protein arginine methyltransferase 5 and nucleolin. *Cancer Res.*, **67**, 10491–10500.
56. Lago,S., Tosoni,E., Nadai,M., Palumbo,M. and Richter,S.N. (2017) The cellular protein nucleolin preferentially binds long-looped G-quadruplex nucleic acids. *BBA - Gen. Subj.*, **1861**, 1371–1381.
57. Juskowiak,B. (2006) Analytical potential of the quadruplex DNA-based FRET probes. *Anal. Chim. Acta*, **568**, 171–180.
58. Xu,H., Zhan,S., Zhang,D., Xia,B., Zhan,X., Wang,L. and Zhou,P. (2015) A label-free fluorescent sensor for the detection of Pb^{2+} and Hg^{2+}. *Anal. Methods*, **7**, 6260–6265.
59. Li,T., Dong,S. and Wang,E. (2010) A lead(II)-driven DNA molecular device for turn-on fluorescence detection of lead(II) ion with high selectivity and sensitivity. *J. Am. Chem. Soc.*, **132**, 13156–13157.
60. Koizumi,M., Akahori,K., Ohmine,T., Tsutsumi,S., Sone,J., Kosaka,T., Kaneko,M., Kimura,S. and Shimada,K. (2000) Biologically active oligodeoxyribonucleotides. Part 12:1 N2-methylation of 2'-deoxyguanosines enhances stability of parallel G-quadruplex and anti-HIV-1 activity. *Bioorganic Med. Chem. Lett.*, **10**, 2213–2216.
61. Virgilio,A., Esposito,V., Citarella,G., Mayol,L. and Galeone,A. (2012) Structural investigations on the anti-HIV G-quadruplex-forming oligonucleotide TGGGAG and Its analogues: evidence for the presence of an A-tetrad. *ChemBioChem.*, **13**, 2219–2224.
62. Stoddart,C.A., Rabin,L., Hincenbergs,M., Moreno,M.E., Linquist-Stepps,V., Leeds,J.M., Truong,L.A., Wyatt,J.R., Ecker,D.J. and Mccune,J.M. (1998) Inhibition of human immunodeficiency virus type 1 infection in SCID-hu Thy/Liv mice by the G-quartet-forming oligonucleotide, ISIS 5320. *Antimicrob. Agents Chemother.*, **42**, 2113–2115.
63. Wyatt,J.R., Davis,P.W. and Freier,S.M. (1996) Kinetics of G-quartet-mediated tetramer formation. *Biochemistry*, **35**, 8002–8008.
64. Oliviero,G., Borbone,N., Amato,J., D'Errico,S., Galeone,A., Piccialli,G., Varra,M. and Mayol,L. (2009) Synthesis of quadruplex-forming tetra-end-linked oligonucleotides: effects of the linker size on quadruplex topology and stability. *Biopolymers*, **91**, 466–477.
65. Oliviero,G., Amato,J., Borbone,N., D'Errico,S., Galeone,A., Mayol,L., Haider,S., Olubiyi,O., Hoorelbeke,B., Balzarini,J. *et al.* (2010) Tetra-end-linked oligonucleotides forming DNA G-quadruplexes: a new class of aptamers showing anti-HIV activity. *Chem. Commun. (Camb).*, **46**, 8971–8973.